Evaluation of a Near-Infrared–Type Contrast Medium Extravasation Detection System Using a Swine Model

Toshihiro Ishihara, RT,† Tatsushi Kobayashi, MD,* Naoya Ikeno, RT,* Takayuki Hayashi, MD,* Masahiro Sakakibara,‡ Noboru Niki, PhD,† Mitsuo Satake, MD,* and Noriyuki Moriyama, MD, PhD§*

Purpose: To refine the development and evaluate the near-infrared (NIR) extravasation detection system and its ability to detect extravasation during a contrast-enhanced computed tomography (CT) examination.

Materials and Methods: The NIR extravasation detection system projects the NIR light through the surface of the human skin then, using its sensory system, will monitor the changes in the amount of NIR that reflected, which varies based on absorption properties.

Seven female pigs were used to evaluate the contrast media extravasation detection system, using a 20-gauge intravenous catheter, when injected at a rate of 1 mL/s into 4 different locations just under the skin in the thigh section. Using 3-dimensional CT images, we evaluated the extravasations between time and volume, depth and volume, and finally depth and time to detect.

Results: We confirmed that the NIR light, 950-nm wavelength, used by the extravasation detection system is well absorbed by contrast media, making changes easy to detect. The average time to detect an extravasation was 2.05 seconds at a depth of 2.0 mm below the skin with a volume of 1.3 mL, 2.57 seconds at a depth between 2.1 and 5 mm below the skin and a volume of 3.47 mL, 10.5 seconds for depths greater than 5.1 mm and a volume of 11.1 mL. The detection accuracy was significantly deteriorated when the depth exceeded 5.0 mm (Tukey-Kramer, $P < 0.05$)

Conclusions: The extravasation system detection system that is using NIR has a high level of detection sensitivity. The sensitivity enables the system to detect extravasation at depths less than 2 mm with a volume of 1.5 mL and at depths less than 5 mm with a volume of 3.5 mL. The extravasation detection system could be suitable for use during examinations.

Key Words: computed tomography, contrast media, contrast-enhanced CT, extravasation detection

(*J Comput Assist Tomogr* 2014;38: 285–292)

It is common during computerized tomography (CT) examinations for the intravenous injection of contrast media to be performed using an automated power injector (injector). The injector provides the flexibility, consistency, accuracy, and safety precautions necessary to perform the required high speed and pressure injections for CT examinations to obtain clinically acceptable images. With this, however, comes the risk of contrast medium extravasation, which requires careful attention.[1] Wang et al [3,4] reported that, in 69,657 patients who were injected with intravenous contrast medium (CM), 475 patients (0.7%) experienced extravasation, and Chew [3,4] determined that the occurrence of extravasation was 0.45%, applying the Self-Assessment Module Scenario 1 by checking previous reports of extravasation after CM injection.[3,4]

Early symptoms of extravasation include local inflammation, sharp pain, and redness of the skin; however, later and more severe extravasations can result in the destruction of tissue. This comes about because of the difference in osmotic pressure between CM and human blood and body fluids. Although it is considered that the toxicity of nonionic contrast media is generally mild, the osmotic pressure is twice that of body fluids. Therefore, a large volume of extravasated CM may cause critical conditions such as ulcer formation or compartment syndrome.[5–14] In addition, the workflow is disrupted, examination efficiency is decreased, plus the reputation of the facility is negatively affected.[14]

Nelson et al [16,17] report an extravasation detection accessory (EDA) that used strain gauges connected (4 points) in a Wheatstone bridge configuration. This system detects the impedance change under a patch measuring 5 × 8 cm and indicates extravasation when a change limit value is exceeded. It was reported this EDA kept 100% sensitivity for 10-mL extravasations. Bouton et al [18] report an extravasation detection accessory that uses radiofrequency. This system detects the change of conductivity using its 4 radiofrequency transmitter/receiver modules surrounding the puncture point. The average volume of the sensing area is 12.5 mL, and it was reported that the system could detect extravasations from 8 to 10 mL.

Hereinafter we shall focus on the extravasation detection system that uses near-infrared (NIR) light. This system uses the absorption characteristics of NIR light by the CM, monitoring the changes of absorption of the scattered NIR light just under the skin.[18–20]

For our evaluation, 7 swine models were used to simulate the extravasation of contrast media inside the thigh skin and evaluate the duration, depth, and volume of extravasation to demonstrate the effectiveness of the system.

MATERIALS AND METHODS

Contrast Media Extravasation Detection System

Overview of the System

The contrast media extravasation detection system consists of 3 parts: a sensor part that includes an alarm box to indicate when contrast media is extravasating, a receiver, and a computer (Windows XP; Dell) that is used to analyze the signal. The configuration is shown in Figure 1. The sensor part detects the intensity changes of the scattered light illuminated into the skin compared with the base intensity that is measured before the

From the *Department of Radiology, National Cancer Center Hospital East; †Graduate School of Functional Systems Engineering, The University of Tokushima; ‡Nemoto Kyorindo Co., Ltd.; and §Research Center for Cancer Prevention and Screening, National Cancer Center, Japan.

Received for publication May 30, 2013; accepted September 9, 2013.

Reprints: Toshihiro Ishihara, RT, Department of Radiology, National Hospital Organization Saitama National Hospital, 2-1, Suwa, Wakho city, Saitama, 351-0102, Japan (e-mail: tishihar@hotmail.com; tishihar@wakho.hosp.go.jp).

T. Ishihara is now with the National Hospital Organization Saitama National Hospital. N. Ikeno is now with the National Hospital Organization Disaster Medical Center. M. Sakakibara is now with Mono Well-being Co., Ltd.

This work was supported in part by the Grant-in-Aid for Cancer Research (21S-1) from the Ministry of Health, Labour and Welfare.

The summary of this study was announced in the 2010 annual meeting of European Society of Radiology.

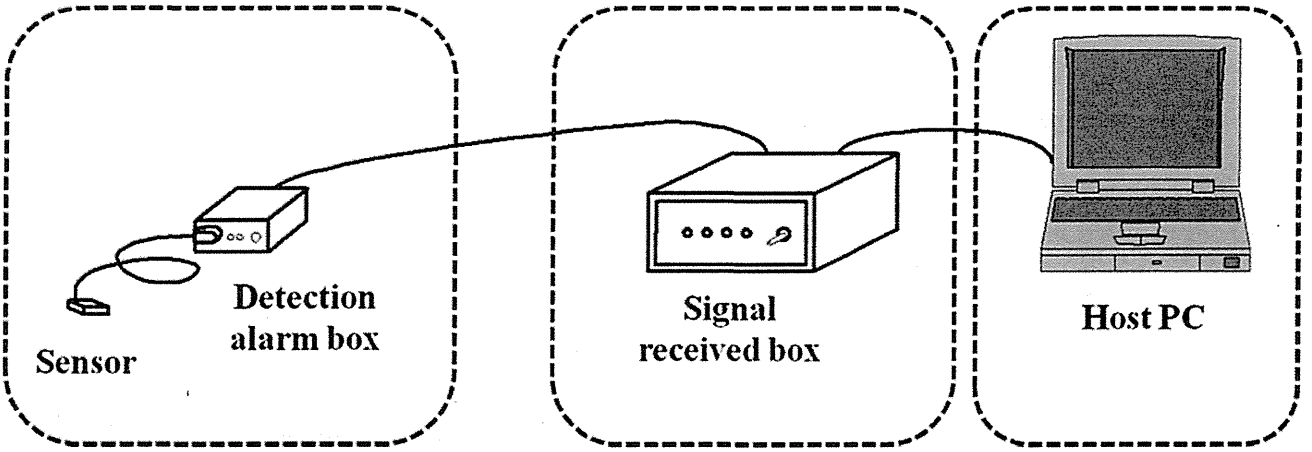

FIGURE 1. Extravasation detection system block diagram. The system is composed of three parts: the calculation unit, the box for receiving (including the box leak detector contrast medium), the leak-detecting sensor signal, the signal sensing, and the signal received. Device used to perform a spectral analysis of the reflected light.

injection. These intensity changes are converted and measured as a change in voltage. When an extravasation occurs, the voltage signal from the sensor part will decrease. Once the voltage decreases below the lower limit, the system will signal an alarm. The computer displays the voltage fluctuation as a trend graph.

Contrast Media Extravasation Detection Sensor

Determination of Light-Absorption Characteristics of Human Skin

Using the diffuse reflectance method, the light-absorption characteristics of human skin around the median cubital vein were measured. For the light source, an incandescent lamp (GA-30H; ELPA) was used because it has a wide optical spectrum. A spectrometer (InGaAs NIR Spectrometer EPP-2000; StellartNet) was used to measure the reflected light. The measuring device is shown in Figure 2. To obtain a baseline for the total reflected light intensity, the incandescent lamp was directed to a white board maintained at a distance of 50 mm and the reflected light was measured. The lamp was then shaded with a black board, and another measurement was made to determine the reflected amount with 100% absorption. Finally, we directed the lamp toward human skin and measured the scattered light. Compared with the total reflected light possible, we confirmed that the option spectrum was 600 to 1000 nm (Fig. 3).

Determination of Absorption Characteristics of Water and Contrast Media

To determine the absorption characteristics of water and contrast media, we used the transmit method. Again, the incandescent lamp was used for the light source and the spectrometer was used to measure the light. Tools were used to prevent the ambient light from affecting our measurements of characteristics of water and contrast media. The measurement system is shown in Figure 4. To determine the absorption characteristics, the lamp was placed on one side of the spectrometer the other side of the

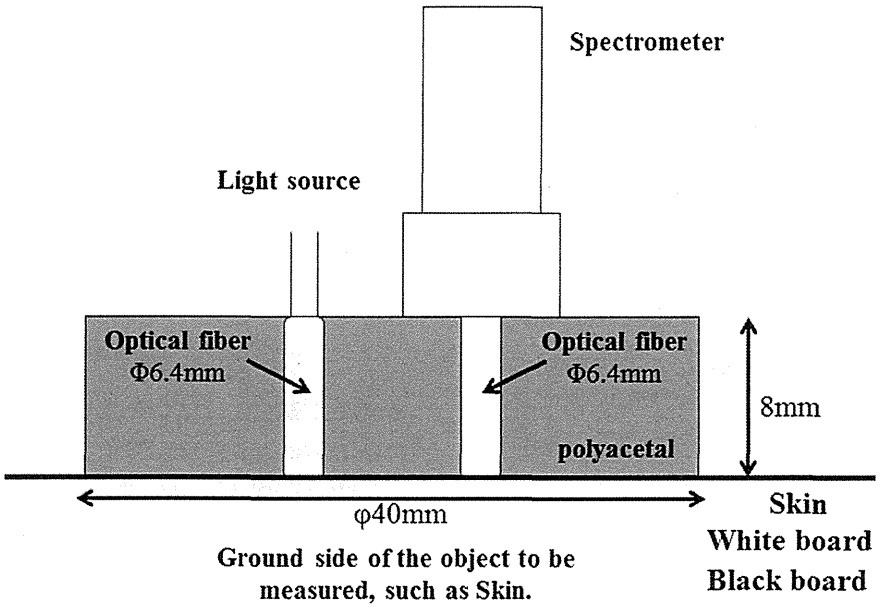

FIGURE 2. Diagram. Detector to measure the light absorption characteristics. Measuring the light absorption characteristics of the reflected light.

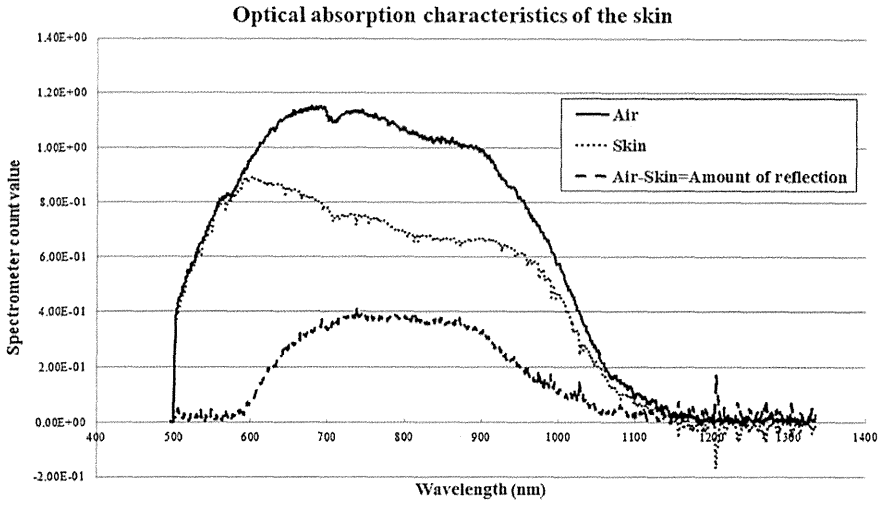

FIGURE 3. The spectrum of light reflected was measured at 600 to approximately 1000 nm for human skin compared with total reflection of light in the air.

water and contrast media. The absorption spectrum band was specifically identified at 950 nm wavelength (Fig. 5). It was determined from these results that a wavelength of 950 nm is ideal to permeate and scatter in the human skin and provide adequate changes based on the absorption by water and contrast media.

Configuration of Contrast Media Extravasation Detection Sensor

For the contrast media extravasation detection sensor, NIR LED (AN1111R; Stanley) having a peak wave length of 950 nm was used for light source and NIR phototransistor (PS1101WA; Stanley) was used for the detector.

The configuration is shown in Figure 6.

The contrast media extravasation detection sensor emits light at a wavelength of 950 nm, NIR, into the human skin, then a measurement of the intensity of reflected light intensity is made using the phototransistor. Comparing the reflected light intensity before injection with the intensity of reflected light during the contrast media injection makes the detection of extravasation possible. If a sufficient amount is absorbed, then an extravasation is suspected and reported.

Determination of Measurement Point of Swine Model

The National Cancer Research Center Animal Study ethics committee and ethics committee of the institute approved this study using animals for data collection of human subjects.

A location with similar hardness and absorption characteristics with the upper median cubital vein of humans for intravascular contrast enhancement CT examination was chosen in the swine model (Specific Pathogen–Free).

The skin hardness was measured on the upper median cubital vein with 6 volunteers (2 women, 4 men; age range, 28–43 years; mean age, 34 years; body mass index range, 17.8–27.6 kg/m^2; mean body mass index, 22.8 kg/m^2) and the 5 points were the abdomen and outer thigh and inner thigh of both legs of 2 swine models (body weight, 30.2 and 31.5 kg).

Skin hardness was measured with a durometer (ASTM D 2240, GS754H, TypeOO Durometer; Teclock Ltd., Okaya, Japan). Three measurements were made then averaged to determine the skin hardness. Note that the hardness measurement is a relative physical amount and has no units of measure. In addition, the absorption characteristics were also measured in the same location, again 3 times then averaged, using the measuring equipment shown in Figure 2 to determine the absorption characteristics.

Evaluation With Swine Model

Simulate an extravasation on 7 swine models and evaluate the performance of contrast media extravasation detection system.

1. The puncture area was chosen based on having similar skin hardness and absorption characteristics as the upper median cubital vein of our human skin measurements. A 20-gauge intravenous catheter (Terumo) was inserted by a physician, and the depth of insertion was adjusted to 1.0 to 10.0 mm. The extravasation detection sensor was placed such that the center of the sensor was positioned 5 mm from the catheter tip and light source. Refer to Figure 7.
2. To set the baseline, the light intensity level before the injector was measure and recorded via the computer. A contrast injection via a power injector (Dual Shot; Nemoto Kyorindo, Tokyo, Japan) was performed at a rate of 1.0 mL/s. The light intensity was observed and compared with that of the baseline during the injection. The contrast media was Iohexal 300 that was diluted 3 times with saline to decrease the influence of artifact.
3. The physician stopped the injection when the light intensity level exceeded the limit. After the injection was stopped, the detection duration and the volume of extravasation were determined.
4. After the extravasation was detected, an image via CT scanner (Aquilion 4; Toshiba Medical Systems, Ootawara, Japan) of the injected area along with the sensor still applied was completed (Fig. 8).

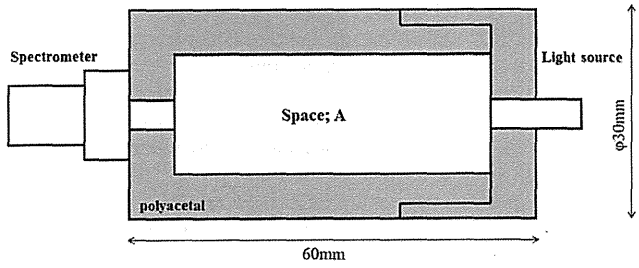

FIGURE 4. Measuring devices for light absorption characteristics of the contrast medium, water, and air. Used to eliminate the effect of ambient light shielding.

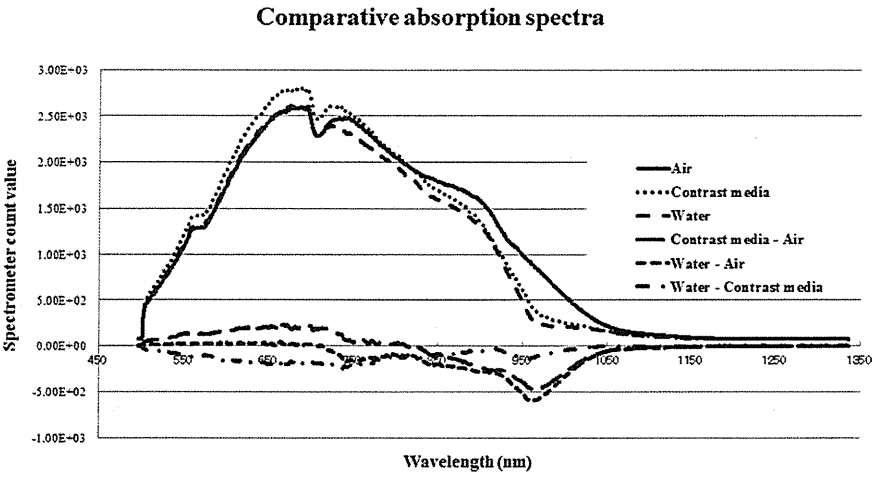

FIGURE 5. Absorption spectrum of the contrast medium with water, which absorbs light at a wavelength of 950 nm specifically, as compared with that passed through air.

Imaging condition of CT was 120 kV, 400 mA, 0.5 sec/rotation speed; low slice thickness, 1.0 mm; pitch factor, 0.875; image slice thickness, 1.0 mm.

5. The depth of the extravasated contrast media was measured using the CT images. Using the profile curve of the CT value, we obtained the distance between the sensor surface on the skin and edge of contrast media. The depth measurement from the skin surface was defined using the full width at 10 maximum (FWTM) of profile curve.

RESULTS

Determination of Measuring Point and the Result of the Swine Model

Skin hardness of human and swine model was measured by the durometer, as shown in Tables 1, 2. The average of skin hardness around the cubital vein was 45.4, and its SD was 0.82. The inside thigh skin of 2 swine models, average was 45.4 and SD was 0.28. Similar skin hardness between inside thigh skin of swine model and cubital vein of human is shown.

Absorption characteristics of cubital vein and inside thigh skin of swine model are shown in Figure 9. Each absorption characteristics shown is in the range of 600 to approximatey 1000 nm, demonstrating similar characteristics.

Result of Swine Model Examination

The relation between the detection duration, depth of extravasation, and extravasated volume for total 28 points of the 7 swine models and 4 points of inside thigh skin are shown in Figure 10A, B.

Figure 10A shows the difference of the extravasated volume compared with the detection time.

A minimum extravasated volume (0.9 mL) could be detected in 2.0 seconds. A shorter detection duration shows a lower extravasated volume. Detection duration and leakage volume were classified into 3 groups (detection duration: group I, 0–3 seconds; group II, 3.1–6 seconds; group III, 6.1–16 seconds). Extravasated volume was 0.9 mL in a detection duration of 2.0 seconds and the average was 3.7 mL in group I; average volume was 8.8 mL in an average detection duration of 5.2 seconds in group II; in group III, the maximum volume was 13.0 mL in 15.0 seconds and the average volume was 13.0 mL in an average duration 14.0 seconds. Correlation between detecting duration and volume were $R^2 = 0.85$, and a positive correlation is shown. When applying the statistical test (Tukey-Kramer), no significance difference was shown between groups I and II; however, comparing group III with groups I and II showed a significant difference because $P < 0.05$. It is also shown that a longer detection time causes an increase in extravasated volume.

Figure 10B shows the difference between the extravasated volumes compared with the depth of extravasation. A minimum extravasated volume (0.9 mL) could be detected in extravastion depths of 0.98 mm. A deeper extravasation leads to an increase in extravasation volume. The depth of extravasation and leakage volume were classified into 3 groups (depth: group I, 0–2.0 mm; group II, 2.1–4.2 mm; and group III, 4.3–10.2 mm); extravasated volume was 0.9 mL in a depth of 0.98 mm and the average was 1.1 mL in group I, average volume was 3.1 mL in group II and the average volume was 6.9 mL. Correlation between detecting duration and volume was $R^2 = 0.85$, and a positive correlation is

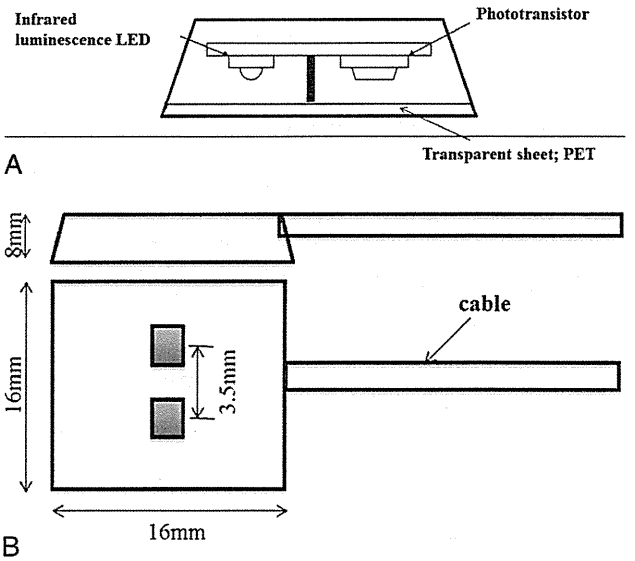

FIGURE 6. Diagram sensor head. Using a phototransistor (Stanley AN1111R), you place the sensor structure (PS1101WA Stanley) LED with infrared emission peak wavelength of 950 nm onto the light source.

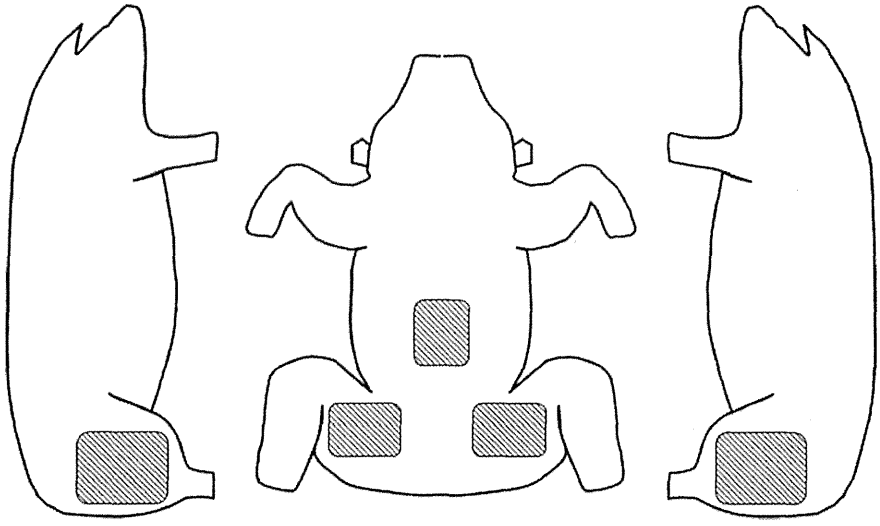

FIGURE 7. Summary installing the sensor in the swine model.

shown. When applying the statistical test (Tukey- Kramer), no significance difference is shown in groups I and II; however, comparing group III with groups I and II shows a significant difference because $P < 0.05$. It is also shown that the delay of detection duration increases with extravasated volume.

The leak positions were classified into 6 groups in accordance with their depths (group I, within 1 mm; group II, 1.1–2.0 mm; group III, 2.1–3.0 mm; group IV, 3.1–4.0 mm; group V, 4.1–5.0 mm; and group VI, 5.1 mm or more), and the average leak volume and average detection time in each leak depth group were compared.

In the case of group II, it was possible to detect within a detection time of 2.1 seconds or less with a leak volume of 1.32 mL or less. In the case of group III, it was possible to detect under within 2.7 seconds or less with a leak volume of 2.7 mL or less. However, in the case of group III, the detection time was 10.5 seconds and the leak volume was 11.1 mL, which showed a remarkable increase. In the multiple simultaneous hypotheses testing (Tukey-Kramer), no significant differences were observed in the leak volumes in I to IV ($*P < 0.05$), but a significant difference was observed in I to VI ($*P < 0.05$), II to VI ($*P < 0.05$), III to VI ($*P < 0.05$), IV to VI ($*P < 0.05$), V to VI ($*P < 0.05$). Regarding the detecting duration, no significant differences were observed in I to IV, significant differences were observed in I to VI ($*P < 0.05$), II to VI ($*P < 0.05$), III to VI ($*P < 0.05$), IV to VI ($*P < 0.05$), and V to VI ($*P < 0.05$) (Fig. 11). As for the contrast medium extravasation detection system, no false-positives or false-negatives were identified. From the above results, extravasation volume could be detected in 1.3 mL in 2.0 mm, and 3.5 mL in 5.0 mm could be detected, and high detection sensitivity was shown.

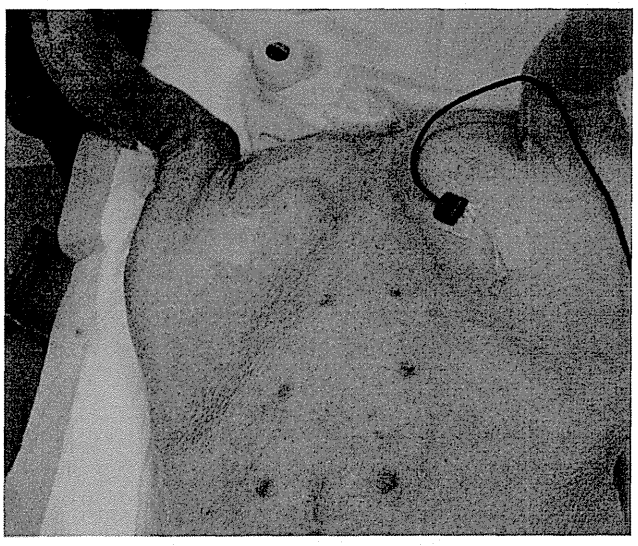

FIGURE 8. CT image showing extravasation in the swine model. The contrast medium accumulated in the right inner thigh.

DISCUSSION

We developed the contrast extravasation detection system, discussed the detection accuracy, and examined the detection performance during an intravenous contrast-enhanced CT examination using a swine model.

The detection accuracy of the contrast detection system that used NIR is high, and an extravasated volume of 1.3 mL could be detected at 2.0 mm depth, and 3.5 mL could be detected within the depth of 5.0 mm. The correlation between the leakage volume and the leakage point showed that deeper extravasations result in increases in the extravasation volume. As for detection accuracy of the contrast medium extravasion detection system, it was confirmed that a deeper contrast medium

TABLE 1. Cubital Vein Measurements in 6 Volunteers

	Human		
Volunteer	Sample No.	Hardness	Part
A	1	45.1	Elbow
B	4	46.4	Elbow
C	7	44.8	Elbow
D	10	46	Elbow
E	13	44.2	Elbow
F	16	45.7	Elbow
Average: Elbow		45.36667	
SD: Elbow		0.816497	

The average hardness of the skin was 45.4 ± 0.82.

TABLE 2. Search Results for 5 Hardness Measurements of the Human Body at the Same Level as the Upper Cubital Vein Swine Model of 2 Animals

Swine Model			
Pig	Sample No.	Hardness	Part
x	1	45.2	Rt. thigh on inside
	2	46.4	Lt. thigh on inside
	3	69.3	Rt. thigh on outside
	4	60.2	Lt. thigh on outside
	5	50.1	Abdomen
y	6	44.8	Rt. thigh on inside
	7	45.3	Lt. thigh on inside
	8	70.5	Rt. thigh on outside
	9	63.4	Lt. thigh on outside
	10	52.7	Abdomen
Average: Thigh on inside		45.425	
SD: Thigh on inside		0.2828427	
Average: Thigh on outside		63.4	
SD: Thigh on outside		4.8802322	
Average: Abdomen		51.4	
SD: Abdomen		1.8384776	

The skin of the inner thigh hardness was 45.4 ± 0.28.

leak position resulted in a longer detection time. There was a correlation between the leakage depth and the leakage volume.

Especially, for example, a leak depth of 5.1 mm or more resulted in a detection time of 10.5 seconds or more. Comparing this with a leakage depth of 5.0 mm or less, the leakage volume significantly increased. It was suggested, however, that there

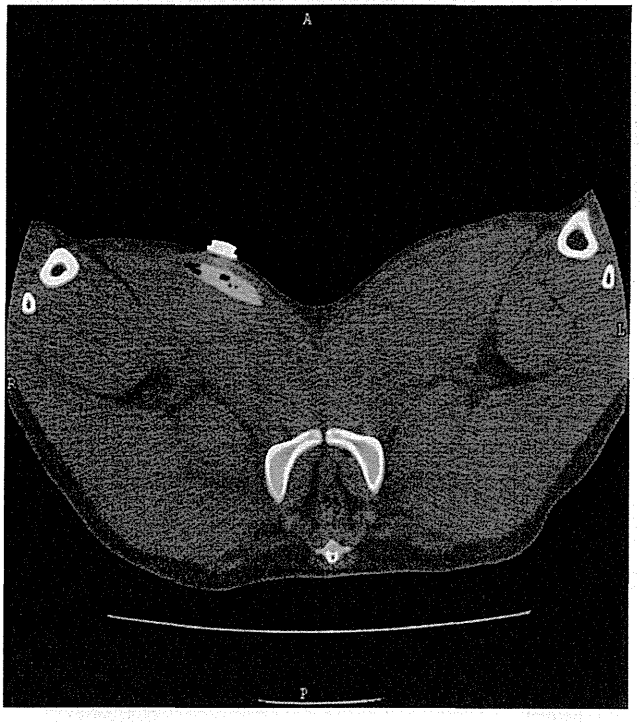

FIGURE 9. Comparing the average value of the absorption characteristics of the pig and the human body. Light absorption characteristics are equivalent.

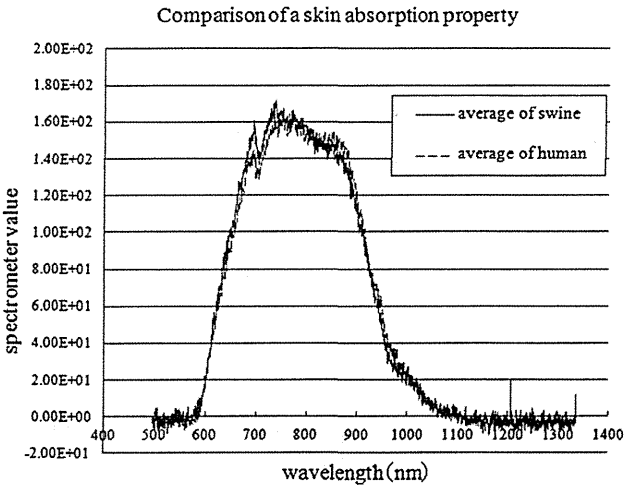

FIGURE 10. A, Relationship between the amount of time and leakage detection. Leakage increases with the increase of leakage detection time. B, Relationship between the amount of leakage and leakage position. Leakage increases with increasing depth of the leak position.

may be several opportunities to improve the device wherein detecting deeper extravasations more accurately would become possible. There is an adequate correlation to the natural logarithm to the depth, detection level, and the transmission loss of light that could enable variations in the operating algorithms to be considered. It was also shown that the rise time of the injection until the flow rate setting is achieved is directly related to the mechanical accuracy of the injector; therefore, mechanical improvements are possible. Finally, testing with human subjects

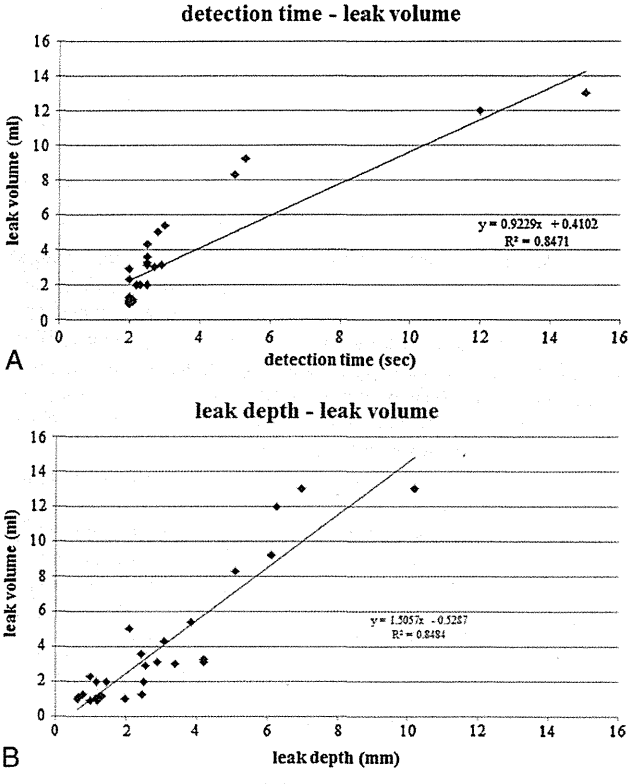

FIGURE 11. Comparison of the amount of leakage and the detection time.

would help in determining the detection influences that were caused by the puncture point resistance by using the swine model. Furthermore, the delay time from when the sensor detects extravasation until the injection stops is influenced by the systems configuration and human factors. From this delay time, the injection volume can be calculated; therefore, improving the system response time can reduce the injected volume before the injection stops.

Based on the results, the contrast medium extravasation detection system could prevent serious diseases such ulcer formation and compartment syndrome by detecting extravasations at their early stage if used at clinical sites. The contrast medium extravasation detection system, if used in the clinical setting, could decrease the probability of occurrence of compartment syndrome with its ability to detect extravasation early and minimize the extravasated amount of contrast. Sistrom et al [22] classified the amount of extravasation into 3 groups (minor, <10 mL; moderate, 10–49 mL; major, ≥50 mL) plus related each group to the damage.

Clinically, it is generally accepted that the contrast medium leak volume, from which the subject feels pain, is about 5.0 to 10 mL. Our newly developed contrast medium extravasation detection system can detect extravasation of about 1 mL and allows stopping injection of the contrast medium before the subject feels pain. Moreover, when the contrast medium extravasation detection system is interfaced with the injector and contrast medium extravasation is detected, it is possible to stop the contrast medium injection automatically. Therefore, interconnecting the two systems is highly recommended, if not indispensable.

It should be noted though, with the sensor tip set close to the tip of the catheter needle, there might be a case that the contrast medium extravasation occurs in the area where the sensor cannot detect it. Therefore, it is necessary to properly install the sensor, noting the effective range of the sensor.

In this study, the injection flow rate of the contrast medium was 1.0 mL/s, but at present, many facilities perform CT examinations at higher flow rates (3.0–5.0 mL/s) that heightens the risk of extravasation.[23–25] However, Jacobs et al [26] propose that there is no correlation to the contrast medium injection flow rate and frequency of extravasation. As for the relation between injection flow rate and contrast medium extravasation, further investigation is needed, taking into account the patients' age and sex, a punctured blood vessel, the catheter needle size, and so on. However, if the flow rate of contrast medium increases, the leak volume per unit time increases. Therefore, the relation between the contrast medium extravasation detection system detection speed and the contrast medium injection flow rate needs further consideration. This study was also limited to only Japanese patients, and although good results were obtained, additional factors, for example, the skin thickness, skin color, hardness, and thickness of the hypodermis should be considered for further study.

There are several advantages that can be considered by using the contrast medium extravasation detection system in everyday CT examinations. For example, incommunicable patients such as small children including infants, the elderly, sedated, or unconscious patients, wherein the injection could be stopped automatically for even small volumes of extravasation. Early detection could also prevent the critical side effects before they occur.

Furthermore, by preventing ulcer formation and compartment syndrome, the system contributes to mitigate the mental burden and minimizes the medical treatment time on the side of our medical staff as well as patients when extravasations occur.

Paice [15] reported in *Imaging Economics* ("extravasation," an analysis that the economical effect due to the extravasation with considering the criticality of the damage and the reparation for injury) the economic impact of an extravasation. It is necessary to prevent the economical loss even with a low probability of occurrence, according to Paice. Also, the occurrence of an extravasation, because of its interruption of the CT examination, decreases the CT department efficiency, along with an adverse impact on the reputation of the hospital.

Often, monitoring with x-rays is performed shortly after the start of a contrast medium injection (eg, bolus tracking method, etc.), medical staff must evacuate from the examination room to avoid being exposed to radiation. However, before leaving the room, they must ensure that the complete dose was injected to the patient.

Therefore, to prevent the risk of contrast medium extravasation, operators take the risk of being exposed to radiation. If, however, the contrast medium extravasation detection system is used, it is possible to avoid unnecessary radiation.[26–30] Sometimes, contrast medium extravasation occurs after the medical staff has confirmed proper puncture, catheter insertion, and left the imaging room. In this situation, it is difficult to decide whether to stop the contrast medium injection or to continue. However, if extravasation is detected with the contrast medium extravasation detection system, the medical staff can be assured that extravasation really occurred, and the injection can be stopped automatically without the medical staff being exposed to radiation.

Developing a system to detect contrast medium extravasation during an intravenous CT imaging examination plays an important role in securing higher levels of safety and reliance on the examinations. Moreover, if the injector and contrast medium extravasation detection system are manufactured by the same manufacturer as the injector, it makes it possible to interconnect systems, providing a solution for minimizing extravasations. This detection system was developed by joint research with the injector manufacturer. Therefore, our detection system provides a high level of safety to the clinical sites.

CONCLUSIONS

The detection accuracy was verified with similar absorption characteristics of human cubital vein and the swine model. The contrast medium extravasation detection system using NIR to detect contrast medium extravasation occurrence could detect within 2 seconds at depths of 2.0 mm or less and a leak volume of 11.1 mL in 10.5 seconds at the maximum depth of 10.2 mm under the skin. Early detection of extravasation at volumes of 3.5 mL at the depth of 5 mm could decrease the risk of serious extravasation.

REFERENCES

1. Schaverien MV, Evison D, McCulley SJ. Management of large volume CT contrast medium extravasation injury: technical refinement and literature review. *J Plast Reconstr Aesthet Surg*. 2008;61:562–565.
2. Wang CL, Cohan RH, Ellis JH, et al. Frequency, management, and outcome of extravasation of nonionic iodinated contrast medium in 69,657 intravenous injections. *Radiology*. 2007;243:80–87.
3. Chew FS. Extravasation of iodinated contrast medium during CT: self-assessment module. *AJR Am J Radiol*. 2010;195:S80–S85.
4. Antebi A, Herscovici D Jr. Acute compartment syndrome of the upper arm: a report of 2 cases. *Am J Orthop*. 2005;34:498–500.
5. Dhawan V, Borschel GH, Brown DL. Acute exertional compartment syndrome of the forearm. *J Trauma*. 2008;64:1635–1637.
6. Upton J, Mulliken JB, Murray JE. Major intravenous extravsation injuries. *Am J Surg*. 1979;137:497–506.

7. Burd DAR, Santis G, Milward TM. Severe extravasation injury: an avoidable introgenic disaster. *Br Med J.* 1985;290:1579–1580.
8. McAlister WH, Palmer K. The histologic effects of four commonly used media for excretory urography and an attempt to modify the response. *Radiology.* 1971;99:511–516.
9. Cohan RH, Leder RA, Bolick D, et al. Extravascular extravasation of radiographic contrast media: effects of conventional and low-osmolar agents in the rat thigh. *Invest Radiol.* 1990;25:504–510.
10. Kim SH, Park JH, Kim YI, et al. Experimental tissue damage after subcutaneous injection of water soluble contrast media. *Invest Radiol.* 1990;25:678–685.
11. McAlister WH, Kissane JM. Comparison of soft tissue effects of conventional ionic low osmolar ionic and nonionic iodine containing contrast material in experimental animals. *Pediatr Radiol.* 1990;20:170–174.
12. Spitany H, Koltz PF, Mays C, et al. CT contrast extravasation in the upper extremity: strategies for management. *Int J Surg.* 2010; 8:384–386.
13. Bellin MF, Jakobsen JA, Tomassin I, et al. Contrast medium extravasation injury: guidelines for prevention and management. *Eur Radiol.* 2002;12:2807–2812.
14. Paice T. Economic Impact of an Extravasation: An Analysis. *Imaging Economics.* 2007.
15. Nelson RC, Anderson FA Jr, Birnbaum BA, et al. Contrast media extravasation during dynamic CT: detection with an extravasation detection accessory. *Radiology.* 1998;209:837–843.
16. Birnbaum BA, Nelson RC, Chezmar JL, et al. Extravasation detection accessory: clinical evaluation in 500 patients. *Radiology.* 1999;212:431–438.
17. Bouton CE, Lombardi T, Hobson FR, et al. Experimental detection of subcutaneous contrast extravasation using radio frequency permittivity sensing. *J Comput Assist Tomogr.* 2009;33:824–7.
18. Ishihara T, Kobayashi T, Ikeno N, et al. Development of innovative contrast medium extravasation detection system for intravenous imaging CT examinations. *ECR.* 2010; Scientific exhibit 10-E-971-ECR.
19. Kashima S, Nishihara M, Kondo T, et al. Model for measurement of tissue oxygenated blood volume by the dynamic light scattering method. *Jpn J Appl Phys.* 1992;31:4097–4102.
20. Vegfors M, Lindberg LG, Oberg PA, et al. Accuracy of pulse oximetry at various haematocrits and during haemolysis in an in vitro model. *Med Biol Eng Comput.* 1993;31:135–141.
21. Sistrom CL, Gay SB, Peffly L. Extravasation of iopamidol and iohexol during contrast-enhanced CT: report of 28 cases. *Radiology.* 1991;180:707–710.
22. Tublin ME, Tessler FN, Cheng SL, et al. Effect of injection rate of contrast medium on pancreatic and hepatic helical CT. *Radiology.* 1999;210:97–101.
23. Kim T, Mrakami T, Takahashi S, et al. Pancreatic CT imaging: effects of different injection rates and doses of contrast material. *Radiology.* 1999;212:219–225.
24. Han JK, Choi BI, Kim AY, et al. Contrast media in abdominal computed tomography: optimization of delivery methods. *Korean J Radiol.* 2001;2:28–36.
25. Jacobs JE, Birbaum BA, Langlotz CP, et al. Contrast media reactions and extravasation: relationship to intravenous injection rates. *Radiology.* 1998;209:411–416.
26. Cohan RH, Bullard MA, Ellis JH, et al. Local reactions after injection of iodinated contrast material: detection, management, and outcome. *Acad Radiol.* 1997;4:711–718.
27. Harmon BH, Berland LL, Lee JY. Effect of varying rates of low-osmolarity contrast media injection for hepatic CT: correlation with iodocyanine green transit time. *Radiology.* 1992;184:379–382.
28. Kopka L, Rodenwaldt J, Fisher U, et al. Dual-phase helical CT of the liver. *Effects of bolus tracking and different volumes of contrast material. Radiology.* 1996;201:321–326.
29. Dinkel HP, Fieger M, Knupffer J, et al. Optimizing liver contrast in helical liver CT: value of a real-time bolus-tracking technique. *Eur Radial.* 1998;8:1608–1612.
30. Bae Kyongtae T. Test-bolus versus bolus-tracking techniques for CT angiographic timing. *Radiology.* 2005;236:369–370.

JOURNAL OF SURGICAL RESEARCH XXX (2014) 1–9

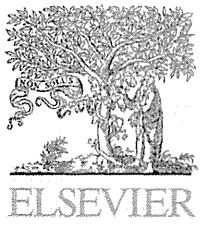

Available online at www.sciencedirect.com

ScienceDirect

journal homepage: www.JournalofSurgicalResearch.com

Pancreatic perfusion data and post-pancreaticoduodenectomy outcomes

Motokazu Sugimoto, MD, PhD,[a,b] *Shinichiro Takahashi, MD, PhD,*[a,*] *Tatsushi Kobayashi, MD,*[c] *Motohiro Kojima, MD, PhD,*[b] *Naoto Gotohda, MD, PhD,*[a] *Mitsuo Satake, MD,*[c] *Atsushi Ochiai, MD, PhD,*[b] *and Masaru Konishi, MD*[a]

[a] *Department of Hepatobiliary-Pancreatic Surgery, National Cancer Center Hospital East, Kashiwa, Chiba, Japan*
[b] *Division of Pathology, Research Center for Innovative Oncology, National Cancer Center Hospital East, Kashiwa, Chiba, Japan*
[c] *Department of Radiology, National Cancer Center Hospital East, Kashiwa, Chiba, Japan*

ARTICLE INFO

Article history:
Received 30 September 2014
Received in revised form
10 November 2014
Accepted 26 November 2014
Available online xxx

Keywords:
Pancreatic CT perfusion
Postoperative pancreatic fistula
Pancreaticoduodenectomy
Fibrosis

ABSTRACT

Background: Precise risk assessment for postoperative pancreatic fistula (POPF) after pancreaticoduodenectomy (PD) may be facilitated using imaging modalities. Computed tomography perfusion (CTP) of the pancreas may represent histologic findings. This study aimed to evaluate the utility of CTP data for the risk of POPF after PD, in relation to histologic findings.

Methods: Twenty patients who underwent preoperative pancreatic CTP measurement using 320-detector row CT before PD were investigated. Clinicopathologic findings, including CTP data, were analyzed to assess the occurrence of POPF. In addition, the correlation between CTP data and histologic findings was evaluated.

Results: POPF occurred in 11 cases (grade A, 6; grade B, 5; and grade C, 0). In CTP data, both high arterial flow (AF) and short mean transit time (MTT) were related to POPF occurrence ($P = 0.001$, $P = 0.001$). AF was negatively correlated with fibrosis in the pancreatic parenchyma ($r = -0.680$), whereas MTT was positively correlated with fibrosis ($r = 0.725$). AF >80 mL/min/100 mL and MTT <16 s showed high sensitivity, specificity, positive predictive value, and negative predictive value (80.0%, 100.0%, 100.0%, and 83.3%, respectively) for the occurrence of POPF.

Conclusions: CTP data for the pancreas were found to be correlated with the occurrence of POPF after PD. Alterations in the blood flow to the remnant pancreas may reflect histological changes, including fibrosis in the pancreatic stump, and influence the outcome after PD. CTP may thus facilitate objective and quantitative risk assessment of POPF after PD.

1. Introduction

Soft pancreatic consistency has traditionally been regarded as a definite risk factor for postoperative pancreatic fistula (POPF) after pancreaticoduodenectomy (PD); however, the consistency is assessed intraoperatively in a subjective and qualitative manner [1–3]. On the other hand, objective and quantitative assessment of POPF risk using preoperative imaging modalities, such as computed tomography (CT) or magnetic resonance imaging (MRI), have been increasingly reported [4–8].

* *Corresponding author.* Department of Hepatobiliary-Pancreatic Surgery, National Cancer Center Hospital East, 6-5-1 Kashiwa-no-ha, Kashiwa, Chiba 277 8577, Japan. Tel.: +81 4 7133 1111; fax: +81 4 7131 4724.
E-mail address: shtakaha@east.ncc.go.jp (S. Takahashi).

0022-4804/$ – see front matter © 2014 Elsevier Inc. All rights reserved.
http://dx.doi.org/10.1016/j.jss.2014.11.046

Computed tomography perfusion (CTP) is a functional imaging technique that is used to assess hemodynamic changes in an organ, and its utility in the diagnosis of cerebrovascular and coronary artery disease has been widely reported [9,10]. In 1995, Miles *et al.* [11] demonstrated the feasibility of absolute quantification to assess blood perfusion in the pancreas for the first time. Subsequently, circulatory alterations were reported in patients with acute or chronic pancreatitis [12–14]. A new generation of CT systems with 320-detector rows offers significant advantages over conventional multidetector CT. Using 320-detector row CT, volumetric acquisition over a range of 16 cm can be achieved with single-rotation scanning, with acceptable image quality and relatively low radiation exposure [15–18]. Therefore, this technique makes it possible to obtain perfusion data of the entire pancreas by performing only one dynamic volume scan with the administration of a single contrast material bolus.

A few studies have reported the clinical utility of CTP of the pancreas using 320-detector row CT. Kandel *et al.* [15] have stated that the perfusion of pancreatic carcinomas is significantly lower than that of normal pancreatic tissue. In hepatic CTP imaging, parameters obtained using CTP have been reported to be correlated with fibrotic changes in liver biopsy specimens [19,20]. Therefore, CTP data may reflect the histologic findings for the specific organ. However, to our knowledge, no such comparison of CTP data with histologic findings has been reported for the pancreas. The aims of the present study were to evaluate the correlations between preoperative CTP data and the incidence of POPF after PD as well as with histologic findings.

2. Material and methods

2.1. *Patients and clinical data collection*

Between March 2012 and February 2013, 20 patients who were scheduled to undergo PD were prospectively recruited for preoperative CTP examination at the National Cancer Center Hospital East, Japan. All patients were examined by preoperative contrast-enhanced multidetector row CT focusing on the lesion, as part of the diagnostic workup; subsequently, PD was indicated for suspected malignancy. CTP was then performed in patients from whom written consent was obtained. Clinicopathologic data were reviewed from medical records. This study was approved by the Institutional Review Board of the National Cancer Center.

2.2. *Surgical techniques and preoperative management*

Details of the surgical maneuvers and preoperative management have been mentioned in our previous article [21]. Subtotal stomach-preserving PD [22] and modified Child reconstruction were performed in all cases. End-to-side pancreaticojejunostomy with the placement of a 6Fr internal short stent through the main pancreatic duct (MPD) was performed as a two-layered anastomosis using interrupted duct-to-mucosa sutures, with coverage of the entire cut surface of the pancreas by the seromuscular layer of the jejunum. Pancreatic consistency was evaluated subjectively as soft or hard by the surgeon during the operation. The definition of POPF was based on the classification of the International Study Group on Pancreatic Fistula [23].

2.3. *Acquisition and interpretation of CTP data*

Patients were examined using a 320-detector row CT (Aquilion ONE; Toshiba Medical Systems Corporation, Ohtawara, Japan). Slices for CTP were selected from precontrast abdominopelvic helical scans and included images as large as an entire pancreas. For CTP, 60 mL of a nonionic contrast material (Iohexol, Ioverin 350; Teva Pharma Japan Inc, Nagoya, Japan) was administered at a rate of 3.5 mL/s with a power injector (Dual Shot GX; Nemoto Kyorindo, Tokyo, Japan), followed by a 40-mL saline bolus. All dynamic CTP images were acquired with the following parameters: 0.5 mm slice thickness, 320 slices, 512 × 512 matrix, 100 kV, 60 mA, and 0.5 s gantry rotation time. The scans were performed 23 times during 6–180 s after injection of the contrast material under quiet breathing. The effective radiation dose for this protocol was 9.72 mSv. Misregistrations due to respiration and automatism were compensated automatically by the Body Registration software (Toshiba Medical Systems) on the console. Regions of interest (ROIs) were placed on the abdominal aorta at the level of the celiac axis, liver, and pancreas to generate time-density curves. Three different ROIs were then placed in the remnant pancreas (body and tail) on both axial and coronal CTP slices, and arterial flow (AF) (mL/min/100 mL) and mean transit time (MTT) (s) were measured at each ROI using the compartment model [24,25] using the Body Perfusion software (Toshiba Medical Systems). ROIs in the pancreas were made as large as possible while avoiding large vessels. Intermediate values for AF and MTT using the median of three ROIs in the axial and coronal slices were analyzed as the CTP data. Examples of two representative cases are shown in Figure 1A–D,E–H. All radiological analyses were performed by an experienced radiologist (T.K.), who was blinded to the operative outcomes and other clinicopathologic findings.

2.4. *Histologic evaluation*

Histological evaluation was performed as described in our previous article [26]. Formalin-fixed, paraffin-embedded specimens obtained from a pancreatic stump were cut into 3-μm thick serial sections. The sections were stained with hematoxylin and eosin (HE) to assess the area of the entire cut surface and MPD; azan-Mallory (azan) stain, to assess the degree of fibrosis; and anti-CD31 antibodies, to assess vessel number and density. Anti-CD31 immunohistochemical staining was performed automatically using a Ventana BenchMark ULTRA (Ventana Medical Systems, Tucson, AZ). Monoclonal anti-human CD31 antibody (Dako, Glostrup, Denmark) was used at a dilution of 1:200, and the conditions for antigen retrieval and primary antibody incubation were set at 95°C for 8 min and 35°C for 60 min, respectively. The slides were photographed using a NanoZoomer Digital Pathology virtual slide viewer (Hamamatsu Photonics, Hamamatsu, Japan) and subjected to morphometric analysis. Histologic analysis of the two cases for which CTP images are presented in Figure 1 A–D,E–H are shown in Figures 2 and 3. Morphometric analysis was performed as described in our previous article [26], and the details of the procedure are outlined in the

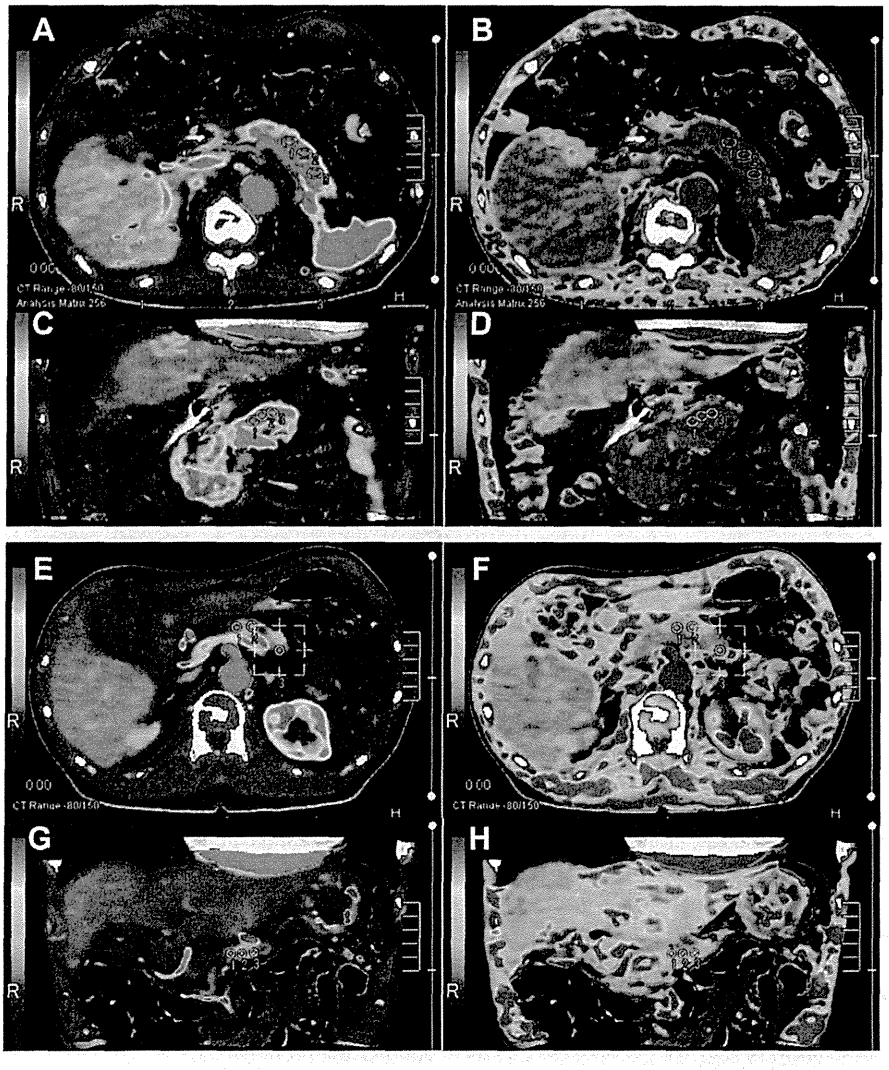

Fig. 1 – (A–D). Acquisition of CTP data for the remnant pancreas in Case 1; a 71-y-old male whose pancreas was intraoperatively palpated as soft, underwent PD for bile duct cancer and developed grade B POPF. CTP images: AF of axial slice (A), MTT of axial slice (B), AF of coronal slice (C), and MTT of coronal slice (D). Three different ROIs were placed in the remnant pancreas (body and tail) on the axial and coronal slices of CTP image. Average data for AF and MTT between the median of the three ROIs in the axial and coronal slices were 110.1 mL/min/100 mL and 9.0 s, respectively. (E–H). Acquisition of CTP data for the remnant pancreas in Case 2; a 70-y-old male with a hard pancreas who underwent PD for pancreatic adenocarcinoma and had an uneventful postoperative course. CTP images: AF of axial slice (E), MTT of axial slice (F), AF of coronal slice (G), and MTT of coronal slice (H). Average data for AF and MTT between the median of the three ROIs in the axial and coronal slices were 37.1 mL/min/100 mL and 43.0 s, respectively. (Color version of figure is available online.)

legends of Figures 2 and 3 in this article. One investigator (M.Su.) carried out all the histologic analyses under the supervision of an experienced pathologist (M.Koji.).

2.5. *Statistical analysis*

Univariate analysis was performed to compare preoperative patient characteristics, CTP data, pancreatic consistency, and histologic findings in the pancreatic stump between patients who did and did not develop POPF (grade A, B, or C). Categorical variables are summarized as numbers and percentages and were evaluated using chi-square test, whereas continuous variables are presented as median ± standard deviation and were evaluated using Mann–Whitney *U* test. Correlations between CTP data and clinicopathologic findings were evaluated using Spearman correlation coefficient *r*. All *P* values were based on two-sided statistical tests; the significance level was set at 0.05. All statistical analyses were performed using SPSS Statistics software (version 19.0; SPSS, Chicago, IL).

3. Results

3.1. *Relationship between clinicopathologic factors and POPF*

PD was performed for eight patients with pancreatic adenocarcinoma, three patients with bile duct cancer, three patients

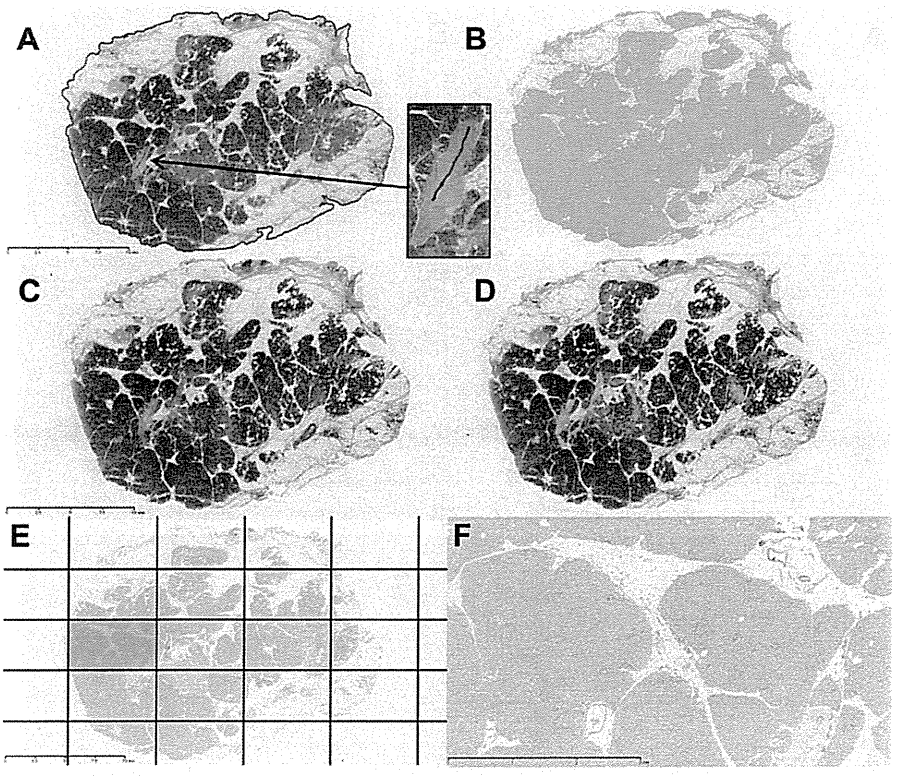

Fig. 2 – Histologic evaluation of the pancreatic stump in Case 1. (A) Loupe image of a HE-stained slide. The arrow indicates a magnified view of the MPD. The outer circumference of the entire cut surface (red line) and the inner circumference of the MPD lumen (blue line) were automatically outlined, and these areas were calculated using the tracing algorithm of the WinROOF software (version 6.5; Mitani Corporation, Tokyo, Japan). The area of the entire cut surface (within the red line) was 411.1 mm^2 and the MPD area (within the blue line) was 0.012 mm^2. The MPD ratio was 0.003%, calculated as the percentage area of MPD in the entire cut surface. (B) The HE-positive area was determined as the visualized area stained with HE using the color-detecting algorithm of the software and identified as bright green in this image. The area of fat was defined as the area of the entire cut surface minus the MPD area and the HE-positive area. The fat ratio was 36.3%, calculated as the percentage area of fat in the entire cut surface. (C) Azan-Mallory (azan) staining was evaluated on the loupe image to determine the degree of fibrosis. (D) The fibrosis area was defined as the visualized area stained with aniline blue using the color-detecting algorithm of the software and identified as bright green in this image. The fibrosis ratio was 2.4%, calculated as the percentage area of fibrosis in the entire cut surface. The lobular area was defined as the HE-positive area minus the MPD area and the fibrosis area. The lobular ratio was 61.3%, calculated as the percentage area of lobules in the entire cut surface. (E) Loupe image of immunohistochemical staining for CD31. The field was divided to allow separate evaluation on the magnified image. (F) Immunohistochemical staining for CD31 at ×4.0 magnification in the blue square shown in Figure 3E. The number of vessels was counted in terms of the number of CD31-immunopositive luminal structures visible in each field. The total number of vessels in the entire cut surface was 666, and the vessel density was 1.6/mm^2. (Color version of figure is available online.)

with ampullary cancer, two patients with intraductal papillary mucinous neoplasm, one patient with duodenal cancer, one patient with neuroendocrine tumor, one patient with solid pseudopapillary tumor, and one patient with autoimmune pancreatitis.

POPF occurred in 11 of the 20 patients (International Study Group on Pancreatic Fistula grade A in 6; grade B in 5; and grade C in 0). Table 1 shows the relationship between clinicopathologic factors and the occurrence of POPF. As compared with patients who did not develop POPF, patients who developed POPF showed a higher AF and shorter MTT in the CTP profile, a lower MPD ratio, lower fat ratio, lower fibrosis ratio, higher lobular ratio, and lower vessel density in the histologic assessment of the pancreatic stump. Figure 4 shows a scattergram of the CTP data and outcomes of POPF. A strong negative correlation was observed between AF and MTT ($r = -0.983$).

3.2. *Correlation between clinicopathologic factors and CTP data*

As shown in Table 2, AF was positively correlated with a soft pancreatic consistency, lobular ratio, and area of the entire cut surface, and negatively correlated with the presence of pancreatic adenocarcinoma, MPD ratio, fibrosis ratio, and vessel density. MTT was positively correlated with MPD ratio, fibrosis ratio, vessel density, and negatively correlated with a soft pancreatic consistency, lobular ratio, and area of the

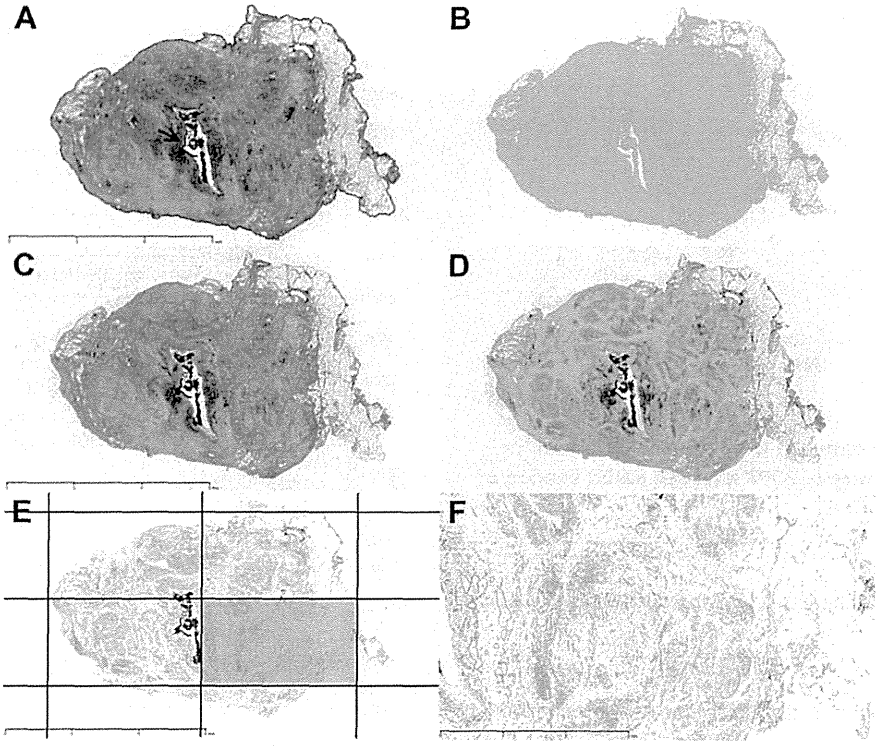

Fig. 3 – Histologic evaluation of the pancreatic stump in Case 2. (A) Loupe image of a HE-stained slide. Arrow indicates the MPD. The area of the entire cut surface (within the red line) was 101.7 mm^2, and the MPD area (within blue line) was 1.091 mm^2. The MPD ratio was 1.073%. (B) The fat ratio was 15.4%. (C) Azan-Mallory-stained slide in the loupe image. (D) The fibrosis ratio was 33.7%. The lobular ratio was 50.6%. (E) Loupe image of immunohistochemical staining for CD31. (F) Immunohistochemical staining for CD31 at ×4.0 magnification in the blue square shown in Figure 5E. The vessel density was 6.0/mm^2. (Color version of figure is available online.)

entire cut surface. Among the histologic features of the pancreatic stump, the fibrosis ratio was most strongly correlated with both AF and MTT ($r = -0.680$ and $r = 0.725$, respectively). POPF occurrence and the correlation between CTP data and the fibrosis ratio are shown in Figure 5. Moreover, a higher fibrosis ratio was correlated with a harder pancreatic consistency ($r = 0.609$), higher MPD ratio ($r = 0.686$), lower lobular ratio ($r = 0.690$), higher vessel density

Table 1 – Risk factor analysis for POPF after PD.

Variable	POPF ($n = 11$)	No POPF ($n = 9$)	P
Age	66 (27–82)	73 (50–80)	0.137
Sex (male %)	8 (72.7)	6 (66.7)	0.769
BMI (kg/m^2)	21.9 (20.3–30.5)	21.2 (18.3–27.6)	0.342
Diabetes, %	2 (18.2)	2 (22.2)	0.822
Pancreatic adenocarcinoma, %	3 (27.3)	5 (55.6)	0.199
CTP data			
AF (mL/min/100 mL)	107.0 (51.3–136.9)	37.1 (25.3–76.4)	0.001*
MTT (sec)	12.4 (7.9–24.0)	43.0 (16.9–63.1)	0.001*
Soft pancreatic consistency, %	9 (81.8)	4 (44.4)	0.081
Histological data			
MPD ratio (%)	0.102 (0.003–1.509)	0.578 (0.038–2.316)	0.030*
Fat ratio (%)	11.5 (7.2–36.3)	25.2 (12.2–44.4)	0.037*
Fibrosis ratio (%)	3.0 (1.1–11.3)	13.8 (2.5–33.7)	0.009*
Acinar gland ratio (%)	85.5 (61.3–89.3)	62.2 (30.4–85.3)	0.007*
Vessel density (mm^2)	1.1 (0.5–2.7)	2.1 (0.9–6.0)	0.017*
Area of entire cut surface (mm^2)	286.0 (157.9–557.4)	205.9 (101.7–374.3)	0.074

BMI = body mass index.
*$P < 0.05$. Differences between the two groups were evaluated using Mann–Whitney U test or chi-square test.

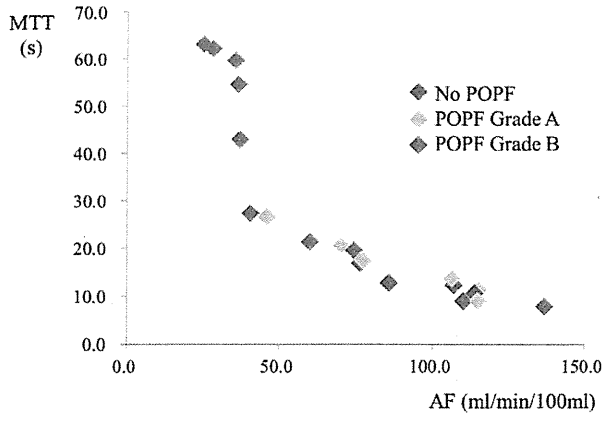

Fig. 4 – Relationship between CTP data for the remnant pancreas and occurrence of POPF after PD. (Color version of figure is available online.)

(r = 0.832), and smaller area of the entire cut surface (r = 0.504).

3.3. *Cutoff value of CTP data for the occurrence of POPF after PD*

Because the CTP data were strongly related to the occurrence of POPF after PD, the cutoff values of AF and MTT were determined using the receiver operating characteristic curve to assess their relationship with POPF. The areas under the receiver operating characteristic curve for the relationship between AF and POPF and between MTT and POPF were 0.949 and 0.939, respectively. When 80 mL/min/100 mL was set as the cutoff value for AF and 16 s as the cutoff value for MTT, the relevant cases were found to be identical. Sensitivity, specificity, positive predictive value, and negative predictive value of AF >80 mL/min/100 mL and MTT <16 s for the occurrence of POPF were 80.0%, 100.0%, 100.0%, and 83.3%, respectively.

Table 2 – Correlation between clinicopathologic factors and CTP data.

Variable	AF	MTT
Age	−0.127	0.140
Sex (male)	−0.265	0.189
BMI	0.015	−0.038
Diabetes	−0.325	0.303
Pancreatic adenocarcinoma	−0.460*	0.442
Soft pancreatic consistency	0.554*	−0.609**
MPD ratio	−0.650**	0.698**
Fat ratio	−0.289	0.250
Fibrosis ratio	−0.680**	0.725**
Lobular ratio	0.484*	−0.465*
Vessel density	−0.570**	0.589**
Area of the entire cut surface	0.484*	−0.552*

BMI = body mass index.
Significant correlations are indicated (*$P < 0.05$, **$P < 0.01$). Correlations between CTP data and clinicopathologic factors were evaluated using Spearman correlation coefficient r.

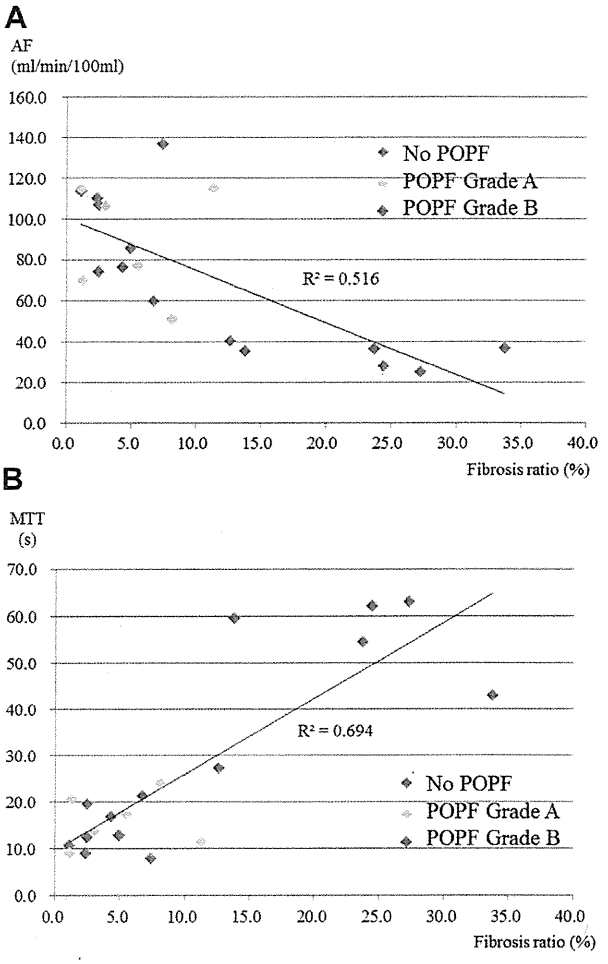

Fig. 5 – (A) POPF occurrence and correlation between AF and fibrosis ratio. (B) POPF occurrence and correlation between MTT and fibrosis ratio. (Color version of figure is available online.)

4. Discussion

In the present study, a high proportion of patients with high AF and short MTT of CTP developed POPF. Both high AF and short MTT were correlated with a soft pancreatic consistency and histologic features such as a lower MPD ratio, lower fibrosis ratio, higher lobular ratio, lower vessel density, and larger area of the entire cut surface. To the best of our knowledge, this is the first study to demonstrate the relationship between CTP data and POPF after PD and the correlation between CTP data and histologic findings. In this study, CTP data acquisition was homogenous and standardized, and the 320-detector row CT made it possible to acquire volumetric CTP data at multiple locations in multiple slices through the entire pancreas. Moreover, histologic evaluation was performed by computer-based automatic analysis. As the utility of morphometric image analysis for immunohistochemical specimens has increasingly been reported [26–29], we were able to estimate the correlation between radiographic and histologic findings in an objective and quantitative manner. This approach may extend our understanding of the

principles involved in the radiological depiction of hemodynamic alterations in the pancreas.

Among other options for predicting POPF after PD involving imaging modalities, the evaluation of the remnant pancreatic volume by preoperative CT or MRI [4], ratio of the pancreatic attenuation value between the hepatic and pancreatic phases as calculated by dual-phase CT [5], time-signal intensity curve of the pancreas obtained from dynamic contrast-enhanced MRI [6,7], and the ratio of signal intensity between the early arterial and portal-venous phases as evaluated by dynamic MRI [8] have been reported to be accurate predictors of POPF after PD. In a dynamic MRI study performed by Tajima *et al.* [7], the time-signal intensity curve profile was correlated with fibrosis of the pancreas, and a relationship between fibrosis and MPD dilation was suggested. In a study of pancreatic CT enhancement patterns, Hashimoto *et al.* [5] demonstrated that the risk of POPF was low in an atrophic, fibrotic pancreas. Likewise, CTP data may be able to predict POPF after PD accurately, as these data reflect histologic changes in the remnant pancreas. In a study of hepatic CTP, Ronot *et al.* [19] noted that MTT was an accurate parameter for differentiating the stages of fibrosis in patients with chronic hepatitis C virus infection.

In the present study, both low AF and prolonged MTT were strongly correlated with increased pancreatic fibrosis. Increased fibrosis was also correlated with a decreased number of pancreatic lobules, increased vessel density, a larger MPD lumen, and a smaller entire cut surface. Marked fibrosis in the pancreas might cause inflow disturbance and prolonged circulation within the organ. Interestingly, low AF was not correlated with decreased vessel density; rather, it showed a correlation with increased vessel density. Increased vessel density might be suggestive of increased neovascularity. Neovascularized microvessels do not contribute to effective blood flow in the organ, and therefore, cause a lower AF and prolonged MTT in such pancreas. Neovascularization, increased fibrosis, decreased lobules, a dilated MPD, and a small amount of pancreatic parenchyma indicate progressive morphologic alterations of the pancreatic parenchyma, consistent with chronic inflammation [26,30–32]. The relationship between these histologic changes and POPF are consistent with the results observed in a previous study by Friess *et al.* [33], who showed that the risk of POPF was low in pancreas with increased fibrosis and decreased exocrine function because of chronic pancreatitis. Therefore, the present study demonstrated that CTP parameters such as low AF and prolonged MTT reflect the progression of fibrosis in the pancreas and are suggestive of a lower risk of POPF.

In a clinical situation, CTP data—as an objective and quantitative parameter—may facilitate more definitive assessment of the risk of POPF after PD, and may allow meaningful comparisons among different institutions and studies, rather than intraoperatively assessed subjective pancreatic consistency. Using preoperative assessment with CTP data, the intraoperative procedures and/or perioperative management can be used as countermeasures for high-risk patients to reduce the incidence of POPF after PD. Recent meta-analyses have reported that reconstruction by pancreaticogastrostomy decreases the rate of POPF after PD in comparison with pancreaticojejunostomy [34,35]. In a recent randomized controlled study, the perioperative use of pasireotide, a somatostatin analog that has a longer half-life than octreotide and a broader binding profile, could reduce the risk and severity of POPF after PD [36]. Precise assessment of POPF risk may thus allow the use of these countermeasures, particularly for high-risk patients.

One of the limitations of this study is the relatively small number of patients included. The cutoff values of AF >80 mL/min/100 mL and MTT <16 s showed a strong relationship to the occurrence of POPF; however, the prognostic impact of CTP data for POPF can be evaluated only after examining data from a large number of patients. Moreover, the CTP data were only assessed using a compartment model for determination of MTT and AF. Comparison with other methods of CTP measurement might be necessary for accurate assessment. Furthermore, although preoperative CTP data were measured in sampled ROIs in the estimated remnant pancreas (body and tail), histologic examination was performed using specimens of the pancreatic cut edge. We assumed that the histologic findings of the pancreatic cut edge might represent the condition of the remnant pancreas.

5. Conclusions

In this preliminary study, high AF and low MTT were related to a high incidence of POPF after PD. These CTP data reflected characteristic histologic features in the pancreas, including low fibrosis, abundant pancreatic lobules, low vessel density, small MPD, and a large area of the entire cut surface, indicating a less-marked effect of chronic inflammation. Therefore, CTP data may enable preoperative, objective, and quantitative assessment of the risk of POPF after PD and allow surgeons to choose appropriate countermeasures against POPF.

Acknowledgment

The authors express special thanks to So Tsushima of the Application Development Group and Shinsuke Tsukagoshi of the CT Systems Development Department of Toshiba Medical Systems Corporation for their technical assistance with 320-detector row perfusion CT. This work was supported in part by Health and Labor Sciences Research grants for Third-term Comprehensive Control Research for Cancer (General-025) and Health and Labor Sciences Research grants for Research on Applying Health Technology.

Authors' contributions: M.Su. had full access to all the data and takes responsibility for data integrity and accuracy of the data analysis. M.Su., S.T., T.K., and M.Koni. contributed to the study concept and design. M.Su., S.T., T.K., M.Koji., N.G., and M.Koni. did the acquisition of data. M.Su., S.T., T.K., and M.Koji. did the analysis and interpretation of data and provided the administrative, technical, and material support. M.Su., T.K., and M.Koji. did the drafting of the article. M.Su., S.T., T.K., M.Koji., A.O., M.Sa., and M.Koni. did the critical revision of the article for important intellectual content.

M.Su., S.T., and T.K. did the statistical analysis. A.O., M.Sa., and M.Koni. did the study supervision.

Disclosure

The authors reported no proprietary or commercial interest in any product mentioned or concept discussed in the article.

REFERENCES

[1] Kawai M, Kondo S, Yamaue H, et al. Predictive risk factors for clinically relevant pancreatic fistula analyzed in 1,239 patients with pancreaticoduodenectomy: multicenter data collection as a project study of pancreatic surgery by the Japanese Society of Hepato-Biliary-Pancreatic Surgery. J Hepatobiliary Pancreat Sci 2011;18:601.
[2] Callery MP, Pratt WB, Kent TS, et al. A prospectively validated clinical risk score accurately predicts pancreatic fistula after pancreatoduodenectomy. J Am Coll Surg 2013;216:1.
[3] Lin JW, Cameron JL, Yeo CJ, et al. Risk factors and outcomes in postpancreaticoduodenectomy pancreaticocutaneous fistula. J Gastrointest Surg 2004;8:951.
[4] Frozanpor F, Loizou L, Ansorge C, et al. Preoperative pancreas CT/MRI characteristics predict fistula rate after pancreaticoduodenectomy. World J Surg 2012;36:1858.
[5] Hashimoto Y, Sclabas GM, Takahashi N, et al. Dual-phase computed tomography for assessment of pancreatic fibrosis and anastomotic failure risk following pancreatoduodenectomy. J Gastrointest Surg 2011;15:2193.
[6] Tajima Y, Kuroki T, Tsutsumi R, et al. Risk factors for pancreatic anastomotic leakage: the significance of preoperative dynamic magnetic resonance imaging of the pancreas as a predictor of leakage. J Am Coll Surg 2006;202:723.
[7] Tajima Y, Matsuzaki S, Furui J, et al. Use of the time-signal intensity curve from dynamic magnetic resonance imaging to evaluate remnant pancreatic fibrosis after pancreaticojejunostomy in patients undergoing pancreaticoduodenectomy. Br J Surg 2004;91:595.
[8] Dinter DJ, Aramin N, Weiss C, et al. Prediction of anastomotic leakage after pancreatic head resections by dynamic magnetic resonance imaging (dMRI). J Gastrointest Surg 2009; 13:735.
[9] Shinohara Y, Ibaraki M, Ohmura T, et al. Whole-brain perfusion measurement using 320-detector row computed tomography in patients with cerebrovascular steno-occlusive disease: comparison with 15O-positron emission tomography. J Comput Assist Tomogr 2010;34:830.
[10] Nasis A, Ko BS, Leung MC, et al. Diagnostic accuracy of combined coronary angiography and adenosine stress myocardial perfusion imaging using 320-detector computed tomography: pilot study. Eur Radiol 2013;23:1812.
[11] Miles KA, Hayball MP, Dixon AK. Measurement of human pancreatic perfusion using dynamic computed tomography with perfusion imaging. Br J Radiol 1995;68:471.
[12] Bize PE, Platon A, Becker CD, et al. Perfusion measurement in acute pancreatitis using dynamic perfusion MDCT. Am J Roentgenol 2006;186:114.
[13] Tsuji Y, Yamamoto H, Yazumi S, et al. Perfusion computerized tomography can predict pancreatic necrosis in early stages of severe acute pancreatitis. Clin Gastroenterol Hepatol 2007;5:1484.
[14] Arikawa S, Uchida M, Kunou Y, et al. Assessment of chronic pancreatitis: use of whole pancreas perfusion with 256-slice computed tomography. Pancreas 2012;41:530.
[15] Kandel S, Kloeters C, Meyer H, et al. Whole-organ perfusion of the pancreas using dynamic volume CT in patients with primary pancreas carcinoma: acquisition technique, post-processing and initial results. Eur Radiol 2009;19:2641.
[16] Goshima S, Kanematsu M, Nishibori H, et al. CT of the pancreas: comparison of anatomic structure depiction, image quality, and radiation exposure between 320-detector volumetric images and 64-detector helical images. Radiology 2011;260:139.
[17] Kanda T, Yoshikawa T, Ohno Y, et al. Perfusion measurement of the whole upper abdomen of patients with and without liver diseases: initial experience with 320-detector row CT. Eur J Radiol 2012;81:2470.
[18] Motosugi U, Ichikawa T, Sou H, et al. Multi-organ perfusion CT in the abdomen using a 320-detector row CT scanner: preliminary results of perfusion changes in the liver, spleen, and pancreas of cirrhotic patients. Eur J Radiol 2012;81:2533.
[19] Ronot M, Asselah T, Paradis V, et al. Liver fibrosis in chronic hepatitis C virus infection: differentiating minimal from intermediate fibrosis with perfusion CT. Radiology 2010; 256:135.
[20] Hashimoto K, Murakami T, Dono K, et al. Assessment of the severity of liver disease and fibrotic change: the usefulness of hepatic CT perfusion imaging. Oncol Rep 2006;16:677.
[21] Sugimoto M, Takahashi S, Gotohda N, et al. Schematic pancreatic configuration: a risk assessment for postoperative pancreatic fistula after pancreaticoduodenectomy. J Gastrointest Surg 2013;17:1744.
[22] Hayashibe A, Kameyama M, Shinbo M, et al. The surgical procedure and clinical results of subtotal stomach preserving pancreaticoduodenectomy (SSPPD) in comparison with pylorus preserving pancreaticoduodenectomy (PPPD). J Surg Oncol 2007;95:106.
[23] Bassi C, Dervenis C, Butturini G, et al. International Study Group on Pancreatic Fistula Definition. Postoperative pancreatic fistula: an international study group (ISGPF) definition. Surgery 2005;138:8.
[24] Ziegler SI, Haberkorn U, Byrne H, et al. Measurement of liver blood flow using oxygen-15 labelled water and dynamic positron emission tomography: limitations of model description. Eur J Nucl Med 1996;23:169.
[25] Materne R, Van Beers BE, Smith AM, et al. Non-invasive quantification of liver perfusion with dynamic computed tomography and a dual-input one-compartmental model. Clin Sci 2000;99:517.
[26] Sugimoto M, Takahashi S, Kojima M, et al. What is the nature of pancreatic consistency? Assessment of the elastic modulus of the pancreas and comparison with tactile sensation, histology, and occurrence of postoperative pancreatic fistula after pancreaticoduodenectomy. Surgery. [In press].
[27] Kojima M, Shiokawa A, Ohike N, et al. Clinical significance of nuclear morphometry at the invasive front of T1 colorectal cancer and relation to expression of VEGF-A and VEGF-C. Oncology 2005;68:230.
[28] Tobin NP, Lundgren KL, Conway C, et al. Automated image analysis of cyclin D1 protein expression in invasive lobular breast carcinoma provides independent prognostic information. Hum Pathol 2012;43:2053.
[29] Aizawa M, Kojima M, Gotohda N, et al. Geminin expression in pancreatic neuroendocrine tumors: possible new marker of malignancy. Pancreas 2012;41:512.
[30] Ammann RW, Heitz PU, Klöppel G. Course of alcoholic chronic pancreatitis: a prospective clinicomorphological long-term study. Gastroenterology 1996;111:224.
[31] Rzepko R, Jaśkiewicz K, Klimkowska M, et al. Microvascular density in chronic pancreatitis and pancreatic ductal adenocarcinoma. Folia Histochem Cytobiol 2003;41:237.

[32] Kuehn R, Lelkes PI, Bloechle C, et al. Angiogenesis, angiogenic growth factors, and cell adhesion molecules are upregulated in chronic pancreatic diseases: angiogenesis in chronic pancreatitis and in pancreatic cancer. Pancreas 1999;18:96.
[33] Friess H, Malfertheiner P, Isenmann R, et al. The risk of pancreaticointestinal anastomosis can be predicted preoperatively. Pancreas 1996;13:202.
[34] Menahem B, Guittet L, Mulliri A, et al. Pancreaticogastrostomy is superior to pancreaticojejunostomy for prevention of pancreatic fistula after pancreaticoduodenectomy: an updated meta-analysis of randomized controlled trials. Ann Surg; 2014 Jun 27.
[35] Xiong JJ, Tan CL, Szatmary P, et al. Meta-analysis of pancreaticogastrostomy versus pancreaticojejunostomy after pancreaticoduodenectomy. Br J Surg 2014;101:1196.
[36] Allen PJ, Gönen M, Brennan MF, et al. Pasireotide for postoperative pancreatic fistula. N Engl J Med 2014;370: 2014.

Eur Radiol
DOI 10.1007/s00330-014-3558-2

INTERVENTIONAL

Retrograde-outflow percutaneous isolated hepatic perfusion using cisplatin: A pilot study on pharmacokinetics and feasibility

Satoru Murata · Shiro Onozawa · Takahiko Mine · Tatsuo Ueda · Fumie Sugihara · Daisuke Yasui · Shin-ichiro Kumita · Mitsuo Satake

Received: 24 May 2014 / Revised: 26 November 2014 / Accepted: 4 December 2014

Abstract
Objectives This study aimed to evaluate the feasibility and underlying pharmacokinetics of the retrograde-outflow technique for percutaneous isolated hepatic perfusion (PIHP).
Methods Retrograde-outflow PIHP was performed in 12 male pigs (weight, 37–44 kg) by redirecting hepatic outflow through the portal vein. Blood with cisplatin (2.5 mg/kg) in an extracorporeal circuit was circulated through the liver under isolation using rotary pumps with balloon catheters. Hepatic angiographic examinations were conducted during perfusion, and histopathological examinations of the organs were conducted after perfusion. The maximum platinum concentration (C_{max}), area under the concentration-time curve (AUC), and chronologic laboratory data were measured.
Results Retrograde-outflow isolated hepatic angiography confirmed that contrast media flowed into the portal veins in all 12 pigs. The hepatic veins and inferior vena cava were not opacified. Hepatic C_{max} (86.3 mg/l) was 39-fold greater than systemic C_{max} (2.2 mg/l), and hepatic AUC (1330.8 min·mg/l) was 30-fold greater than systemic AUC (44.6 min·mg/l). Histopathological examinations revealed no ischaemic changes or other abnormalities in the liver, duodenum, small intestine, or colon. Within 1 week of the procedure, chronologic laboratory data (n=3) normalized or returned to pre-therapy levels.
Conclusions The retrograde-outflow technique appears to enable safe and feasible PIHP therapy.

S. Murata (✉) · S. Onozawa · T. Mine · T. Ueda · F. Sugihara · D. Yasui · S.-i. Kumita
Department of Radiology/Center for Advanced Medical Technology, Nippon Medical School, 1-1-5 Sendagi, Bunkyou-ku, Tokyo, 113-8602, Japan
e-mail: genji@nms.ac.jp

M. Satake
Department of Diagnostic Radiology, National Cancer Center Hospital East, 6-5-1 Kashiwanoha Kashiwa, Chiba, 277-8577, Japan

Published online: 18 December 2014

Key Points
- *The portal vein acted as an outflow tract under retrograde-outflow PIHP.*
- *Plasma hepatic-to-systemic exposure ratio was 39.2 for the maximum platinum concentration.*
- *Plasma hepatic-to-systemic exposure ratio was 29.8 for the AUC.*
- *The retrograde-outflow technique appears to enable safe and feasible PIHP.*

Keywords Liver · Isolation perfusion cancer chemotherapy · Percutaneous · Retrograde · Experimental

Introduction

Several forms of locoregional treatment have been used to manage primary and secondary unresectable liver malignancies. Repeated transcatheter arterial infusion (TAI) therapy yields higher response rates than systemic chemotherapy; however, no convincing evidence of a long-term survival benefit has been found [1–4]. Transcatheter arterial chemoembolization (TACE), a widely used palliative treatment, is based on a high degree of tumour arterialization [5, 6]. However, the effectiveness of transcatheter treatment is reduced by the presence of dual blood supply (i.e., arterial and portal) to hepatic tumours, which makes it impossible to deliver anticancer agents to the entire tumour or to achieve sufficient tumour ischaemia without irreversibly damaging the surrounding non-tumorous parenchyma [7–9].

Several researchers have obtained promising results by using surgically isolated hepatic perfusion (IHP) to overcome this obstacle [10–13]. Isolated perfusion is a method to separate the hepatic circulation from the systemic circulation by occluding both hepatic inflow (the hepatic artery and portal vein) and outflow (hepatic vein), and connecting both to

extracorporeal pumps. Ligation and cannulation of each vessel is performed via laparotomy under IHP. However, this treatment is limited in that it requires an aggressive surgical intervention that is associated with considerable morbidity and mortality. Another limitation of this technique is that it does not allow for repeated intervention, mainly because of the formation of adhesions [10, 12–15]. Because laparotomy is unnecessary, percutaneous IHP techniques using balloon occlusion catheters may potentially result in lower procedural morbidity and shorter operative times. Furthermore, percutaneous IHP techniques with balloon occlusion catheters can enable repeated administration of chemotherapy in the same patient, potentially resulting in greater therapeutic efficacy in the treatment of unresectable liver tumours [16, 17]. IHP utilizes an orthograde approach, by employing the hepatic artery as an inflow route and the inferior vena cava (IVC) through the hepatic veins as an outflow route, similar to the physiologic condition. In previous studies, percutaneous IHP techniques showed higher rates of leakage from the perfusion circuit into the systemic circulation [16–19], mainly because the distance between the origins of the right atrium and the hepatic vein is often too short to allow balloon occlusion of the suprahepatic IVC without occluding the hepatic veins themselves [16, 19] and incompletely occluding the IVC or diaphragmatic veins. All orthograde IHP techniques that employ a double-balloon catheter for IVC occlusion, including combinations of orthograde percutaneous and surgical IHP techniques, may develop increased leakage into the systemic circulation because of this.

In acute segmental hepatic venous outflow occlusion, the corresponding liver parenchyma is supplied only by the artery and drained via the portal vein [20, 21], suggesting that retrograde IHP could be applied by employing hepatic artery inflow and portal vein outflow. Based on this theory, we developed a retrograde-outflow percutaneous IHP circulation system (R-PIHP) by redirecting hepatic outflow through the portal vein. The aim of this study was to evaluate the feasibility and the underlying pharmacokinetics of R-PIHP.

Materials and methods

Animal model

The Animal Experiment Ethics Committee of our university approved all animal experiments. Surgical procedures were performed under sterile conditions and anaesthesia, in 12 male pigs weighing 37–44 kg (mean, 42 kg). A veterinary physician was also involved in the study. The liver of each animal was shown to be morphologically normal by ultrasound examination prior to the procedure. The results of blood studies were within normal limits prior to the procedure.

Systemic circulation monitoring

Peripheral arterial oxygen saturation was maintained at > 95 % and was monitored using a probe that was applied to the ear. Each animal was monitored by electrocardiography throughout the procedures. The left axillary artery and left jugular vein were exposed through cut-down incisions, and a cannula sheath (5-French; Terumo Clinical Co., Ltd., Tokyo, Japan) was inserted into each vessel. The left axillary artery cannula was used to monitor blood pressure during the procedures. The left jugular vein cannula was used to collect blood samples and administer Ringer's solution (Lactec G injection; Otsuka Pharmaceutical Co. Ltd., Iwate, Japan) by intravenous drip infusion.

Catheterization and perfusion techniques

Figure 1 illustrates the techniques used for this study.

Construction of the isolated hepatic circuit

Infusion site: hepatic artery The right common femoral artery was exposed through cut-down incisions, and an 8-French cannula sheath (Medikit Co. Ltd., Tokyo, Japan) was inserted.

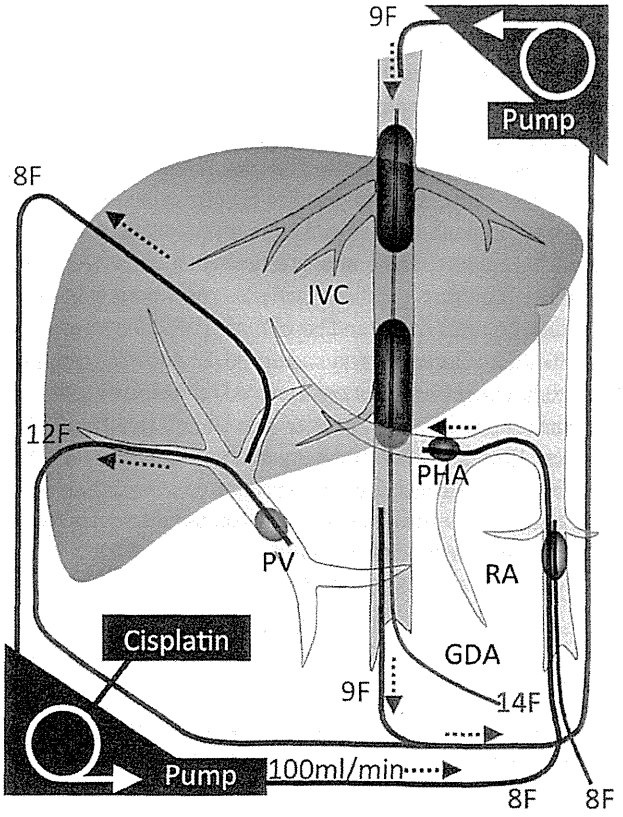

Fig. 1 The technique used for retrograde-outflow isolated hepatic perfusion. IVC, inferior vena cava; PV, portal vein; GDA, gastroduodenal artery; PHA, proper hepatic artery; RA, renal artery

Anterior mesenteric arteriography and celiac arteriography were performed for anatomical mapping. The gastroduodenal artery was embolized with coils to prevent drug leakage. The 8-French balloon catheter (Terumo Clinical Co., Ltd.) was then positioned in the common hepatic artery.

Aspiration site: portal vein Two intrahepatic portal branches were punctured with an 18-gauge percutaneous transhepatic cholangiography needle under ultrasonographic guidance. An 8-French cannula sheath with side holes was inserted into the portal vein to aspirate blood with cisplatin from the intrahepatic portal veins. A 12-French sheath was inserted into the portal vein. After systemic heparinization (120 U/kg), one 12-French cannula sheath with a 35-mm balloon (Forte Co., Ltd., Tokyo, Japan) was placed in the portal vein trunk to aspirate outflow blood via the anterior mesenteric and splenic veins (aspiration pressure at < 100 mm Hg) and return the blood into the jugular vein. This technique offered two advantages for R-PIHP. First, it compensated for decreased systemic venous return. Second, it prevented the inflow of blood via the anterior mesenteric and splenic veins into the intrahepatic portal veins beyond the portal occlusion balloon catheter.

Redirecting the hepatic outflow through the portal vein One 14-French double-balloon catheter with 35-mm balloons (Forte Co., Ltd.) was placed via the right femoral vein into the hepatic portion of the suprarenal vena cava to occlude the hepatic veins.

Perfusion technique The balloon catheters in the hepatic artery, abdominal aorta, portal vein, and IVC were inflated in that order. The abdominal aorta was occluded just below the renal artery to compensate for decreased systemic venous return [22], by using a balloon catheter with a 35-mm balloon (Forte Co., Ltd.) that was inserted via the left femoral artery. After confirming the patency of the R-PIHP system by isolated hepatic arteriography, blood containing cisplatin (Nippon Kayaku Co., Ltd., Tokyo, Japan) was injected into the hepatic artery (injection rate, 100 ml/min) while blood was aspirated from the portal vein (aspiration rate, 100 ml/min) using rotary pumps. The period of R-PIHP therapy was fixed at 30 min. The total liver ischaemia time never exceeded 45 min [16].

Construction of the systemic circuit

Prior to vessel occlusion at each site, blood from the anterior mesenteric and splenic veins was aspirated via the tip of the balloon occlusion catheter in the portal vein trunk by using a rotary pump, while maintaining aspiration pressure at < 100 mm Hg to avoid haemolysis. Another 9-French cannula sheath was inserted into the IVC via the left femoral vein for IVC blood aspiration at a pressure of < 100 mm Hg. The rotary pumps were started after vessel occlusion, and the aspirated blood from each site was returned to the right jugular vein.

Choice of drug and dosage

Many researchers have used alkylating agents, such as melphalan, for the treatment of various types of tumours in IHP [17]; however, melphalan has not been authorized for use in Japan. Therefore, we decided to use cisplatin as a reference drug. The use of a large range of cisplatin doses (from 0.5 mg/kg to 3 mg/kg) [23, 24] has been reported in previous studies on IHP therapies. In the present study, we chose a relatively high cisplatin dose of 2.5 mg/kg body weight, because melphalan content in tumour tissue has been shown to be unaffected with either orthograde or retrograde IHP, although melphalan content in the liver was reduced by 80 % using the retrograde technique [25]. Moreover, an in vivo fluorescent microscopic study in a rat tumour model demonstrated that blood flow in the major portion of the hepatic lobules was stopped during retrograde IHP, with enhancement of only 40.7 % of the liver parenchyma [26].

Measurements and assessments

Effects of R-PIHP on haemodynamics Haemodynamic parameters, arterial blood pressure, and heart rate were measured before, during, and after R-PIHP. None of the pigs received vasopressor agents.

Confirmation of the R-PIHP system Digital subtraction angiography was performed before R-PIHP therapy by the injection of contrast media (300 mg I/ml) into the hepatic artery to confirm the patency of the R-PIHP system. The rotary pumps achieved a perfusion rate of 100 ml/min with the same aspiration rate. Hepatic arteriography was performed using 30 ml of contrast media injected into the hepatic artery and then aspirated from the portal vein. Isolated hepatic arteriography was performed to verify that contrast media flowed only into the liver, with no extrahepatic opacification, and that the contrast media in the liver flowed into the intrahepatic portal vein, and not into the IVC.

Pharmacokinetics of the serum platinum concentration Plasma platinum concentrations were measured in blood samples collected from the hepatic arterial circulation and systemic venous circulation (superior vena cava) before and at 1, 3, 5, 10, 20, and 30 min after beginning R-PIHP. The maximum platinum concentration (C_{max}) and the area under the platinum blood concentration-time curve (AUC) were determined from these data and compared for each site. Plasma samples were digested with nitric acid for analysis of metal species. Platinum concentrations were measured using atomic